NAVAL POSTGRADUATE SCHOOL
Monterey, California

THESIS

A STOCHASTIC MODEL FOR SHOALING WAVES

by

Craig A. Norheim

March, 1997

Thesis Advisor: Thomas H.C. Herbers

Approved for public release; distribution is unlimited.

REPORT DOCUMENTATION PAGE

Form Approved OMB No. 0704-0188

1. AGENCY USE ONLY *(Leave blank)*	2. REPORT DATE	3. REPORT TYPE AND DATES COVERED
	March, 1997	Master's Thesis

4. TITLE AND SUBTITLE	5. FUNDING NUMBERS
A Stochastic Model for Shoaling Waves	
6. AUTHOR(S) Craig A. Norheim	
7. PERFORMING ORGANIZATION NAME(S) AND ADDRESS(ES) Naval Postgraduate School Monterey CA 93943-5000	8. PERFORMING ORGANIZATION REPORT NUMBER
9. SPONSORING/MONITORING AGENCY NAME(S) AND ADDRESS(ES)	10. SPONSORING/MONITORING AGENCY REPORT NUMBER

11. SUPPLEMENTARY NOTES The views expressed in this thesis are those of the author and do not reflect the official policy or position of the Department of Defense or the U.S. Government.

12a. DISTRIBUTION/AVAILABILITY STATEMENT	12b. DISTRIBUTION CODE
Approved for public release; distribution is unlimited.	

13. ABSTRACT *(maximum 200 words)*

Boussinesq-type equations for weakly nonlinear, weakly dispersive waves have been used extensively to model wave shoaling on beaches. Deterministic Boussinesq models cast in the form of coupled evolution equations for the amplitudes and phases of discrete Fourier modes (Freilich and Guza, 1984) describe the shoaling process accurately for arbitrary incident wave conditions, but are numerically cumbersome for predicting the shoaling evolution of continuous spectra of natural wind-generated waves. Here an alternative stochastic formulation of a Boussinesq model (Herbers and Burton, 1996, based on the closure hypothesis that phase coupling between quartets of wave components is weak) is implemented that predicts the evolution of a continuous frequency spectrum and bispectrum of waves normally incident on a gently sloping beach with straight and parallel depth contours. The general characteristics of the model are examined with numerical simulations for a wide range of incident wave conditions and bottom profiles. Stochastic and deterministic Boussinesq model predictions are compared to field observations from a cross-shore transect of bottom pressure sensors deployed on a barred beach near Duck, NC, during the recent DUCK94 Experiment. Predictions of the two models are similar and describe accurately the observed nonlinear shoaling transformation of wave spectra.

14. SUBJECT TERMS Boussinesq Equations, Finite Depth Theory, Ocean Surface Gravity Waves, Nonlinear Interactions, Shoaling, Beach, Wave Model	15. NUMBER OF PAGES 58
	16. PRICE CODE

17. SECURITY CLASSIFICATION OF REPORT	18. SECURITY CLASSIFICATION OF THIS PAGE	19. SECURITY CLASSIFICATION OF ABSTRACT	20. LIMITATION OF ABSTRACT
Unclassified	Unclassified	Unclassified	UL

NSN 7540-01-280-5500

Standard Form 298 (Rev. 2-89)
Prescribed by ANSI Std. 239-18 298-102

Approved for public release; distribution is unlimited.

A STOCHASTIC MODEL FOR SHOALING WAVES

Craig A. Norheim
Lieutenant, United States Navy
A.S., Florida Institute of Technology, 1984
B.S., University of New Mexico, 1990

Submitted in partial fulfillment
of the requirements for the degree of

MASTER OF SCIENCE IN PHYSICAL OCEANOGRAPHY

from the

NAVAL POSTGRADUATE SCHOOL
MARCH 1997

ABSTRACT

Boussinesq-type equations for weakly nonlinear, weakly dispersive waves have been used extensively to model wave shoaling on beaches. Deterministic Boussinesq models cast in the form of coupled evolution equations for the amplitudes and phases of discrete Fourier modes (Freilich and Guza, 1984) describe the shoaling process accurately for arbitrary incident wave conditions, but are numerically cumbersome for predicting the shoaling evolution of continuous spectra of natural wind-generated waves. Here an alternative stochastic formulation of a Boussinesq model (Herbers and Burton, 1996, based on the closure hypothesis that phase coupling between quartets of wave components is weak) is implemented that predicts the evolution of a continuous frequency spectrum and bispectrum of waves normally incident on a gently sloping beach with straight and parallel depth contours. The general characteristics of the model are examined with numerical simulations for a wide range of incident wave conditions and bottom profiles. Stochastic and deterministic Boussinesq model predictions are compared to field observations from a cross-shore transect of bottom pressure sensors deployed on a barred beach near Duck, NC, during the recent DUCK94 Experiment. Predictions of the two models are similar and describe accurately the observed nonlinear shoaling transformation of wave spectra.

TABLE OF CONTENTS

I. INTRODUCTION 1

II. A STOCHASTIC BOUSSINESQ MODEL 7

III. SIMULATIONS 11

IV. COMPARISONS TO FIELD OBSERVATIONS 17

V. SUMMARY AND CONCLUSIONS 23

APPENDIX 27

LIST OF REFERENCES 45

INITIAL DISTRIBUTION LIST 47

ACKNOWLEDGMENT

I express my sincere appreciation to my advisor, Thomas Herbers, for his guidance and many hours of discussion and instruction, without which, this paper would never have come about.

I would also like to thank my wife, Rhonda, for her support, editing assistance and understanding.

I. INTRODUCTION

Wind-generated surface gravity waves are the principal driving force of nearshore fluid motions (e.g., longshore currents, rip currents, and undertow) and sediment transport (e.g., erosion and accretion of beaches, and the formation of bars and cusps). As waves shoal onto beaches, amplitudes increase, wavelengths decrease, and propagation directions refract towards normal incidence. These linear propagation effects are readily observed and well understood. Additionally, pronounced nonlinear effects in shallow water cause a dramatic transformation of wave shapes from initially smooth, nearly sinusoidal profiles, to asymmetric, pitched forward profiles characteristic of near-breaking waves. The mechanism for this transformation is nonlinear triad interactions in which two primary wave components with frequencies ω_1 and ω_2 excite a secondary wave component with the sum $(\omega_1+\omega_2)$ or difference $(\omega_1-\omega_2)$ frequency. The nonlinear energy transfers in these interactions not only broaden the spectrum but also change the statistical properties of the waves. Whereas the primary wave components incident from deep water are approximately statistically independent, the newly formed secondary components are "phase locked" to the primary waves that excite them. Even relatively weak secondary components significantly change the shapes of waves in shallow water. While the incident waves and the nonlinearly excited higher frequency waves are predominantly dissipated in the surf zone, the nonlinearly excited lower frequency (infragravity) wave components reflect from the beach and often dominate wave runup at the shoreline. Accurate prediction of the nonlinear shoaling transformation of waves is critical to both naval (e.g.,

amphibious landings and mine warfare) and civilian (e.g., mitigation of beach erosion) operations in the littoral zone.

In deep water ($\kappa h \gg 1$, where κ is the wavenumber and h is the water depth) and intermediate depths ($\kappa h = O(1)$) triad interactions are non-resonant. The nonlinearly excited secondary waves remain small ("bound" waves) and are well described by finite depth theory based on Stokes perturbation expansion for small wave steepness (Phillips 1960; Hasselmann 1962; Herbers et al., 1992,1994; and many others). In shallow water ($\kappa h \ll 1$), where triad interactions are near-resonant, finite depth theory is valid only for small values of the Ursell number, $U_r = a/\kappa^2 h^3$ (Ursell, 1953) where a is the wave amplitude, and this condition is usually violated on natural beaches.

Models for waves in shallow water are usually based on the Boussinesq equations which assume that a/h (nonlinearity) and $(\kappa h)^2$ (dispersion) are both small and of the same order (i.e., $U_r = O(1)$). These equations are surprisingly robust, even for large U_r values typically observed in near-breaking waves. Peregrine (1967) extended the Boussinesq equations to varying depth, and these equations form the basis of most wave shoaling models. Freilich and Guza (1984) developed a frequency domain (i.e., neglecting directional spreading effects) Boussinesq model that predicts accurately the energy transfers to higher frequencies and associated wave shape changes on natural beaches (Elgar and Guza, 1985a; Elgar et al., 1990a). This deterministic model is initialized at an offshore boundary by a discrete Fourier representation of the incident waves. A coupled set of evolution equations for the amplitudes and phases of the Fourier modes is solved numerically to evaluate the shoaling transformation of the wave train. The results of these

integrations are subsequently averaged over many realizations with random initial amplitudes and phases to obtain spectral statistics. Although the shoaling evolution of wave spectra is accurately reproduced, this method is cumbersome for practical applications, requiring large computing resources and a detailed specification of incident wave conditions at the offshore boundary that is often not available. In addition, the extension of this approach to include directional spreading effects (i.e., two dimensions) is far from straightforward owing to the large number of modes required in discrete mode simulations of continuous frequency-directional wave spectra.

The initialization of wave shoaling models requires local offshore measurements (e.g., wave following buoys) or predictions from a global or regional wind-wave generation model. These larger scale models (e.g., WAM; The WAMDI group, 1988) are typically stochastic formulations based on an energy balance, and predict wave spectra rather than individual wave profiles. Routine measurement systems provide similar statistical information.

Recently, Herbers and Burton (1996) derived an alternative stochastic formulation of Boussinesq shoaling evolution equations, for directionally spread waves propagating over a gently sloping beach with straight and parallel contours. Based on the closure hypothesis that phase-coupling between quartets of wave components is weak, Herbers and Burton derived a coupled set of evolution equations for the wave spectrum and bispectrum. The bispectrum describes the degree of coupling and the phase-relationship in triads of nonlinearly interacting wave components (Hasselmann et. al., 1963), and is used extensively in other nonlinear process studies (e.g., economics, brain-wave emission,

and plasma physics). In deep water and intermediate depths, the bispectrum is completely determined by the local spectrum, and enables the detection of relatively weak phase-coupled, forced secondary waves that are concealed in the spectrum by more energetic freely propagating primary waves (e.g., Herbers et al., 1992, 1994). In shallow water, the bispectrum evolves strongly and describes, in a statistical sense, the shape evolution of shoaling waves (e.g., Elgar and Guza, 1985b; Elgar et al., 1990a).

Here, a numerical implementation of a one-dimensional stochastic Boussinesq model is presented in which directional spreading effects are neglected. This formulation allows for simple illustration of stochastic model characteristics and comparisons to field data and existing one-dimensional models. Energy transfers to higher frequencies in sum triad interactions are insensitive to directional spreading angles of incident waves (e.g., Herbers and Burton, 1996), and thus can be predicted accurately with a one-dimensional model. However, energy transfers to infragravity frequencies in difference triad interactions are significantly reduced for large directional spreading angles (Herbers and Burton, 1996). Additionally, the reflection from shore and refractive trapping of infragravity waves (Herbers et al., 1995) is neglected. Hence, infragravity waves are only crudely represented in the present model formulation.

Following a review of the stochastic formulation of Boussinesq wave shoaling equations, the numerical model implementation is described in Chapter II. The dependence of wave shoaling evolution on the nonlinearity, spectral shape of incident waves and the beach profile is examined through numerical simulations in Chapter III. Stochastic and deterministic (the Freilich and Guza model) Boussinesq predictions are

compared to field data collected on a natural beach near Duck, NC in Chapter IV, followed by conclusions in Chapter V.

II. A STOCHASTIC BOUSSINESQ MODEL

Herbers and Burton (1996) derived a stochastic formulation of Boussinesq wave shoaling equations for directionally spread waves propagating over a beach with straight and parallel depth contours. Under the third-order closure hypothesis that phase-coupling between quartets of wave components is weak, the statistical properties of the waves are described by a coupled set of evolution equations for the frequency (ω)-alongshore wavenumber (l) spectrum $E(\omega,l)$ and bispectrum $B(\omega',l',\omega-\omega',l-l')$. If directional spreading is neglected (i.e., $l = 0$), these equations (22a and 22b in Herbers and Burton, 1996) reduce to:

$$\frac{d}{dx}E(\omega) = -\frac{1}{2h}\frac{dh}{dx}E(\omega) + \frac{3\omega}{2h^{3/2}g^{1/2}}\int_{-\infty}^{\infty} IM\{B(\omega',\omega-\omega')\}d\omega' \qquad (1)$$

$$\frac{d}{dx}B(\omega',\omega-\omega') = \left[-\frac{3}{4h}\frac{dh}{dx} - i\frac{h^{1/2}\omega'(\omega-\omega')\omega}{2g^{3/2}}\right]B(\omega',\omega-\omega') - i\frac{3}{2h^{3/2}g^{1/2}}\left[\omega' E(\omega-\omega')E(\omega)+(\omega-\omega')E(\omega')E(\omega)-\omega E(\omega')E(\omega-\omega')\right] \qquad (2)$$

where the x-axis points onshore, $E(\omega)$ and $B(\omega',\omega-\omega')$ are the frequency spectrum and bispectrum, $h(x)$ is the water depth, g is gravity, and $IM\{\ \}$ indicates the imaginary part. The integrals of the (density) spectrum E and bispectrum B over all frequencies yield the mean square $<\eta^2>$ and mean cube $<\eta^3>$ of the surface elevation $\eta(x,t)$:

$$\langle \eta^2 \rangle = \int_{-\infty}^{\infty} E(\omega) d\omega$$

$$\langle \eta^3 \rangle = \int_{-\infty}^{\infty} \int B(\omega', \omega - \omega') d\omega' d\omega$$

The first term on the right-hand side of equations (1) and (2) represents linear shoaling effects. The nonlinear transfers in the energy spectrum are controlled by the imaginary part of the bispectrum (the integral on the right-hand side of equation (1)). The energy product terms in equation (2) represent the changes in the imaginary part of the bispectrum due to the three possible nonlinear interactions (one sum interaction and two difference interactions) within the (ω',ω-ω',ω) triad. The second term on the right-hand side of equation (2) represents the detuning of the interactions from resonance (i.e., changes in the phase of the bispectrum owing to weak dispersion). In the limit of small amplitudes and bottom slope, steady solutions for $E(\omega)$ and $B(\omega', \omega-\omega')$ smoothly match the second-order bound-wave solutions of dispersive finite depth theory (Herbers and Burton, 1996).

The model is initialized with a spectrum $E(\omega)$ specified at the offshore boundary of the model domain (e.g., from nearby measurements or a regional model prediction) and the corresponding second-order finite depth theory expression for the bispectrum $B(\omega', \omega-\omega')$.

$$B(\omega',\omega-\omega') = 2[D(\omega',\omega-\omega')E(\omega')E(\omega-\omega') + D(\omega',-\omega)E(\omega')E(\omega) + D(\omega-\omega',-\omega)E(\omega-\omega')E(\omega)] \tag{3}$$

The coupling coefficient D is given by

$$D(\omega_1,\omega_2) = \frac{(\omega_1+\omega_2)^2}{g(\kappa_1+\kappa_2)\tanh[(\kappa_1+\kappa_2)h] - (\omega_1+\omega_2)^2} \times \left\{\frac{\omega_1\omega_2}{g} - \frac{g\kappa_1\kappa_2}{\omega_1\omega_2} - \frac{g}{2(\omega_1+\omega_2)}\left(\frac{\kappa_1^2}{\omega_1\cosh^2(\kappa_1 h)} + \frac{\kappa_2^2}{\omega_2\cosh^2(\kappa_2 h)}\right)\right\} + \frac{\omega_1^2+\omega_1\omega_2+\omega_2^2}{2g} - \frac{g\kappa_1\kappa_2}{2\omega_1\omega_2} \tag{4}$$

where h is the local water depth, and the frequencies ω_1, ω_2 and wavenumbers κ_1, κ_2 ($\kappa_i < 0$ for $\omega_i < 0$) of the interacting primary wave components obey the linear theory dispersion relation $\omega_i^2 = g\kappa_i\tanh(\kappa_i h)$(Hasselmann, 1962; Hasselmann et al.,1963).

Using the symmetry relations (Hasselmann et al., 1963):

$$\begin{aligned} E(\omega) &= E(-\omega) \\ B(\omega',\omega-\omega') &= B(\omega-\omega',\omega') = B^*(-\omega',\omega'-\omega) \\ &= B(\omega',-\omega) = B(\omega-\omega',-\omega) \end{aligned}$$

where * indicates the complex conjugate, the integral term in equation (1) can be expressed as the sum of two integrals over positive frequencies

$$\int_{-\infty}^{\infty} IM\{B(\omega',\omega-\omega')\}d\omega' = \int_{0}^{\omega} IM\{B(\omega',\omega-\omega')\}d\omega' - 2\int_{0}^{\infty} IM\{B(\omega',\omega)\}d\omega' \qquad (5)$$

that represent the energy transfers to frequency ω resulting from the sum interaction of frequencies ω', $\omega-\omega'$, and the difference interaction of frequencies $\omega+\omega'$, ω', respectively. Hence integrations of the spectrum and bispectrum evolution equations (1), (2) can be restricted to positive frequencies (ω', $\omega-\omega'$, $\omega > 0$).

The spectrum and bispectrum are discretized:

$$\begin{aligned} \omega_n &= n\Delta\omega \qquad \text{for } n = 1, 2, .., N \\ E_n &= E(\omega_n) \qquad \text{for } n = 1, 2, .., N \\ B_{nm} = R_{nm} + iI_{nm} &= B(\omega_n,\omega_m) \quad \text{for } n = 1, 2, .., N-1 \text{ and } m = 1, 2, .., N-i \end{aligned}$$

where $\Delta\omega$ is the bandwidth and ω_N the highest frequency included in the computations. With these definitions, equations (1) and (2) reduce to a linear set of N^2 ordinary differential equations which can be written in the general form

$$\frac{d\vec{Y}}{dx} = \vec{F}(\vec{Y})$$

where the elements of $\vec{Y}$ are the discretized spectrum (E_n) and bispectrum (R_{nm}, I_{nm}) values and $\vec{F}(\vec{Y})$ incorporates the corresponding right-hand side of equations (1) and (2). This system of equations is solved using the Bulirsch-Stoer method, a variant of Richardson extrapolation to the limit that uses adaptive stepsize control (Press et al., 1992; Bulirsch and Stoer, 1966).

III. SIMULATIONS

To investigate the general model characteristics and the dependence of wave shoaling evolution on the nonlinearity, spectral shape and bottom profile, extensive numerical simulations were carried out with simple incident wave spectra of the general form:

$$E_1(f) = E\frac{n}{f_p}\exp\left(\frac{n}{1-n}\left(\frac{f}{f_p}\right)^{1-n}\right)\left(\frac{f}{f_p}\right)^{-n} \tag{6}$$

$$E_2(f) = E\frac{n}{\pi f_p}\operatorname{sech}\left(n\,\frac{f-f_p}{f_p}\right) \tag{7}$$

where E_1 and E_2 are single-sided spectra ($E(f) = 4\pi E(\omega)$ with $f = \omega/2\pi$), E is the surface elevation variance $\langle\eta^2\rangle$ and the parameter n defines the width of the spectrum. E_1 is a broad spectrum with a power law high-frequency tail characteristic of actively generated wind waves. E_2 has a narrow symmetric exponential shape, characteristic of remotely generated swell. All model simulations were initialized in a depth h = 6 m with a spectral peak frequency f_p = 0.07 Hz. The corresponding wave number κ_p = 0.058 m^{-1} yields a representative value of the dispersion parameter κh = 0.35 at the offshore boundary. Example simulations of the shoaling of a broad sea spectrum (E_1 with n = 5, the Pierson-Moskowitz [1964] spectral shape) and a narrow swell spectrum (E_2 with n = 20, the full

width at half maximum power is 0.009 Hz) are shown in Figures 1-5 for different bottom profiles and incident significant wave heights ($H_s \equiv 4E^{1/2}$). The initial bispectrum was obtained by substituting the initial spectrum in the finite depth theory relation (equation 3).

The shoaling evolution of a narrow swell spectrum with significant wave heights of 0.05 and 0.5 m on plane beaches with slopes of 1:30 and 1:300 is shown in Figure 1. All four simulations show the familiar growth of harmonic peaks at frequencies $2f_p$, $3f_p$, ··· and an infragravity peak at about 0.01 Hz. Even for the small H_s = 0.05 m waves, harmonic spectral levels are significant (up to 10 % of the primary peak level) in 1.5 m depth. Although the nonlinearity remains weak ($[2E]^{1/2} / h$, a representative value of a/h, varies between 0.003 and 0.017), the Ursell number ($U_r = [2E]^{1/2} / \kappa_p^2 h^3$) increases from 0.024 in 6 m depth to a relatively large value of 0.58 in 1.5 m depth. As expected, the shoaling evolution is much stronger for the larger H_s = 0.5 m waves with harmonic spectral levels that are comparable to the primary peak levels in 1.5 m depth. In these simulations a/h increases from 0.03 in 6 m depth to 0.17 in 1.5 m depth, and U_r increases from 0.24 to 5.8. In both the H_s = 0.05 and 0.5 m cases, stronger growth of harmonic and infragravity peaks is predicted on a gentle 1:300 slope than on a steep 1:30 slope. Eventually (Figure 1 d, f) nonlinear energy transfers fill the valleys between harmonic peaks and the spectrum flattens, similar to simulations with a deterministic Boussinesq model reported by Elgar et al. (1990b).

The energy transfers and their dependence on the bottom slope are further illustrated in Figure 2 with normalized bispectrum predictions in 2 m depth. The

normalized bispectrum:

$$b(f_1, f_2) = \frac{B(f_1, f_2)}{\sqrt{E(f_1)E(f_2)E(f_1 + f_2)}} \quad (8)$$

with $B(f_1, f_2) = 8\pi^2 B(\omega_1, \omega_2)$, defined analogous to $E(f)$, indicates a relative measure of phase coupling between frequencies f_1, f_2 and $f_1 + f_2$ (Herbers et al., 1992). Positive values of the imaginary part of the bispectrum indicate energy transfers to higher frequencies through sum interactions, whereas negative values indicate energy transfers to lower frequencies through difference interactions (equations 1, 5). All four simulations show strong coupling at (f_1, f_2) = (0.07, 0.07) Hz associated with the f_p, f_p, $2f_p$ sum interaction and at (0.07, 0.14) Hz (the f_p, $2f_p$, $3f_p$ sum interaction). The larger wave and gentle bottom slope simulations also show coupling to higher harmonics (e.g., the (0.14, 0.14), (0.21, 0.07), and (0.21, 0.14) Hz peaks). Whereas the imaginary part of b is small on the gentle 1:300 slope (i.e., peaked but nearly symmetric wave shapes, Elgar and Guza, 1985) the real part of b is small on the steep 1:30 slope (i.e., pitched forward wave shapes). The energy transfer rate (proportional to the imaginary part of the bispectrum, equation 1) is smaller on the gentle slope than on the steep slope but the longer interaction distances cause stronger cumulative spectral evolution (Figure 1).

Simulation results of the shoaling of a broad spectrum with the same initial significant wave heights (0.05 and 0.5 m) and beach slopes (1:30 and 1:300) are shown in Figure 3. The spectral evolution is much weaker than in the narrow spectra simulations because the principal effect of triad interactions is to spread energy to frequencies where

spectral levels are relatively low. In the H_s = 0.05 m simulations (Figure 3 a, c, e) the nearly uniform increase in spectral levels at frequencies $\gtrsim$ 0.05 Hz is a linear shoaling (decrease in wave group speed) effect (the first term on the right-hand side of equation 1). The 1:300 slope simulation shows slightly larger growth of spectral levels above about $2f_p$ that is the result of sum interactions. The larger wave (H_s = 0.5 m) simulations (Figure 3 b,d,f) show the expected stronger nonlinear evolution. Although the spectrum remains featureless, nonlinear interactions cause a flattening to a nearly white spectrum in 1.5 m depth, similar to the narrow spectrum simulations (Figure 1f). The dependence on bottom slope is qualitatively similar to the narrow spectrum results with larger cumulative energy transfers on a gently sloping beach (compare the solid and dashed curves in Figure 3).

The shoaling evolution of a broad spectrum of waves (initial H_s = 0.5 m) over three different bottom profiles is compared in Figure 4. All three profiles start with a gently sloping (1:300) section from 6 to 3 m depth to let the waves evolve to a shallow water regime with significant nonlinear energy transfers. From 3 m depth shoreward, the waves either continue to shoal on a 1:300 slope to 1 m depth ("beach" case), propagate the same 600 m distance in (constant) 3 m depth ("flat" case), or unshoal over a -1:200 section back to 6 m depth ("bar" case). In contrast to the beach case, the spectral evolution between x = 900 and x = 1500 m is weak over the flat bottom, and on the back side of the bar high frequency spectral levels are reduced to approximately the initial levels in 6 m depth. At infragravity frequencies spectral levels continue to increase on all three profiles, but the growth is strongest on the beach profile and weakest on the bar

profile (Figure 4).

Bispectra after 150 m of evolution on the three different profiles are compared in Figure 5. The predicted small imaginary part of the bispectrum remains positive on the beach profile, allowing for continued energy transfers to high frequencies (equations 1, 5). On the flat bottom where the spectral evolution is weak, the imaginary part of the bispectrum shows small alternating positive and negative peaks. On the negative slope section of the bar profile, positive values of the imaginary part of the bispectrum (i.e., energy transfers to higher frequencies) evolve to negative values (i.e., energy transfers to lower frequencies) over a wide range of frequencies, causing a reversal in nonlinear energy transfers towards lower frequencies (Figure 4).

In simulations of waves propagating over a flat bottom and into deeper water (Figure 4), small undulations are noted in the spectra that grow with distance and eventually develop into instabilities. A sensitivity analysis of the numerical solutions to variations in frequency bandwidth, the error tolerance of the numerical integration routine, the maximum frequency, and using different extrapolation techniques (i.e., polynomial and rational extrapolation), yielded identical features in all calculations. Energy was also conserved in these simulations to a high degree of accuracy. These numerical tests indicate that the predicted growing undulations in the spectrum are true features of the spectral and bispectral evolution equations and not caused by numerical truncation errors. However, the Boussinesq equations, truncated at second-order in nonlinearity and thus valid only over $O(a/h)^{-1}$ wavelengths (Freilich and Guza, 1984), do not describe accurately the longterm evolution of these moderately energetic waves.

Hence, the undulations in the spectrum may not be physically real but possibly result from the breakdown of the weakly nonlinear approximation used in the present model.

IV. COMPARISONS TO FIELD OBSERVATIONS

Extensive field observations of wave shoaling were obtained during the fall of 1994 in the DUCK94 nearshore field experiment (Elgar et al., 1996). A cross-shore transect of 15 SPUV systems, each consisting of a co-located pressure transducer, bidirectional electromagnetic current meter, and sonar altimeter were deployed on a sandy, barred beach near Duck, North Carolina. The 350 m long transect extended from the shoreline to about 6 meters depth (Figure 6). The sample frequency of all instruments was 2 Hz. Sea surface elevation spectra with approximately 120 degrees of freedom were estimated from three-hour-long pressure records using a linear theory depth correction.

The present analysis of four case studies is focused on benign wave conditions (incident wave significant heights ranged from 0.4 - 0.8 m) when the surf zone was confined to the beach face at the shoreward end of the transect. These observations span a 2 week period in September with small bathymetric changes. Differences between the depth profiles of the case studies (Figure 6) are primarily due to tidal sea level fluctuations. The beach profile is characterized by a sandbar located about 120-140 m from the shoreline and submerged approximately 2.2-2.5 m below the mean sea surface. The bottom slope is approximately 1:80 seaward of the sandbar. Shoreward of the sandbar, the profile deepens slightly (20-40 cm) into a relatively flat, 80 m wide trough that extends to the steep (1:10) beach face. The beach profile used in the Boussinesq model computations was obtained through linear interpolation of the depth estimates extracted from the sonar altimeters (Gallagher et al., 1997).

Stochastic Boussinesq model predictions of wave spectrum evolution in the four case studies are compared to the observed spectrum evolution and deterministic Boussinesq model predictions (provided by Dr. Steve Elgar) in Figures 7, 8, 12 and 15. The stochastic model predictions for 15, 21 and 24 September were initialized with the spectrum measured at the furthest offshore pressure sensor, p19. The 10 September case was initialized with pressure sensor p18 because sensor p19 malfunctioned during this run. The deterministic model predictions were initialized with the measured pressure time series (see Elgar et al. 1996 for further details) at the same locations.

In all four cases (and other case studies not shown) predictions of both models are in excellent agreement with the observed wave shoaling evolution. The narrow swell spectrum cases (10 and 15 September) show the familiar amplification of harmonic peaks. On 10 September the incident wave spectrum is dominated by a narrow swell peak (peak frequency $f_p \approx 0.075$ Hz), with a broader, but relatively small sea peak at 0.12 Hz (Figure 7). Energy is transferred from the swell peak frequency f_p to higher frequencies through sum triad interactions resulting in distinct harmonic peaks at $2f_p$ (0.15 Hz; driven by f_p, f_p interactions), $3f_p$ (0.23 Hz; f_p, $2f_p$ interactions) and $4f_p$ (0.3 Hz; f_p, $3f_p$ and $2f_p$, $2f_p$ interactions). Close to shore the small 0.12 Hz incident sea peak is completely submerged in the $2f_p$ swell harmonic (Figure 7f).

On September 15 the incident wave spectrum is distinctly bimodal with a narrow swell peak ($f_p \approx 0.06$ Hz) and a slightly smaller sea peak at twice the swell frequency ($2f_p \approx 0.12$ Hz) (Figure 8). As these wave systems propagate over the shallow sandbar, large nonlinear energy transfers in sum interactions yield clearly distinguishable harmonic peaks

at $3f_p$, $4f_p$ and $5f_p$ (compare Figure 8a and 8c). The cross-shore evolution of spectral levels at frequencies f_p, $2f_p$, $3f_p$, $4f_p$ and $5f_p$ is shown in Figure 9. Partial reflection of the dominant 0.06 Hz swells from the beach is evident in the large cross-shore energy variations (i.e., standing wave patterns) observed close to shore. Good agreement between the observed and predicted growth of higher-frequency harmonics indicates that nonlinear energy transfers are insensitive to weak reflections from shore (Elgar et al., 1996).

Both the observed and predicted bispectra on September 15 show the expected shoaling transition from real values (i.e., skewed but symmetric wave profiles) (Figure 10a and 10b) to imaginary values (i.e., pitched-forward wave profiles) (Figure 10c and 10d). Although the observed and predicted bispectral levels generally agree within the considerable uncertainty in estimates extracted from short field data records (records longer than 3 hours could not be used owing to tide-induced depth changes), they differ in detail at the shallower sites (Figure 11). In frequency pairs involving the 0.06 Hz swell peak, the observed bispectrum shows a dramatic shift from real to imaginary values between sensors p3 and p4 (separated by only 15 m) that is absent in the model results. This biphase shift is caused by the partial reflection of the 0.06 Hz swell from shore (Figure 9) that is not incorporated in the model predictions . Midway between nodes and antinodes (e.g., sensor p4) the reflected components are 90° out of phase with the incident components, causing large biphase shifts in triads involving the standing wave component.

The September 24 spectrum, is broader and more energetic, with a peak frequency, $f_p \approx 0.1$ Hz (Figure 12). Sum interactions transfer energy to a broad range of higher frequencies, causing a broadening of the spectrum rather than the development of distinct

harmonic peaks observed on September 10 and 15. The observed and predicted spectral levels at $3f_p$ decrease sharply between the bar crest (x = 240 m) and the slightly deeper trough (x = 300 m), whereas energy levels at $2f_p$ continue to increase (Figure 13). These results suggest that energy is transferred back to lower frequencies as waves travel over the sandbar into deeper water similar to the simulation results (Figures 4, 5). Observed and predicted bispectra (Figure 14) show a clear transition from positive imaginary parts seaward of the bar crest to negative imaginary parts shoreward of the bar crest at high frequencies that is consistent with this reversal in the nonlinear energy transfer (equations 1, 5).

In contrast to the September 10, 15 and 24 case studies, the shoaling evolution of the broad, featureless spectrum observed on September 21 (Figure 15) is weak even though the nonlinearity is comparatively strong in this case (the incident wave significant height is 0.8 m). Sum and difference interactions cause significant energy transfers, but do not strongly affect the spectrum because the interactions, spread over a wide frequency range, tend to cancel out in a broad spectrum. Predicted bispectral levels (not shown) are low, consistent with the observations.

Discrepancies between the stochastic model predictions and the observations, and between the deterministic model predictions and the observations are roughly comparable (observed and predicted spectral levels generally agree within about a factor of four) but differ in detail. Initially the deterministic model tends to overpredict energy transfers to higher frequencies whereas the stochastic model predictions are in close agreement with the observed spectra (e.g., Figures 7a-c, 8a-b). During the later stages of shoaling

evolution, the stochastic model tends to overpredict high-frequency spectral levels, whereas the deterministic model predictions are close to, or in some cases, underpredict (e.g., Figure 12 c, d) the observed spectral levels. Some of these differences may be the result of the different formulation of dispersion effects in the two models. The stochastic model uses Peregrine's (1967) "consistent" approximation, whereas the deterministic model uses Freilich and Guza's (1984) "dispersive" approximation. Comparisons of deterministic Boussinesq models to field data reported by Freilich and Guza (1984) show similar trends of overprediction (for the "consistent" approximation) and underprediction ("dispersive" approximation) of high frequency spectral levels. Other possible explanations for small differences between the deterministic and stochastic model predictions are the different way the models initialize third-order statistics (the stochastic model uses second-order finite depth theory whereas the deterministic model uses measured time series) and the statistical closure of the stochastic model. Additionally, dissipation (neglected in both models) and higher-order nonlinear effects likely contribute significant errors in the predictions close to shore.

The predicted shoaling amplification of low frequency (<0.06 Hz) spectral levels is generally in reasonable agreement with the observations, even though the model is obviously inadequate at infragravity frequencies. It is well known that reflection from shore (e.g., Elgar et al., 1994) and refractive trapping in deeper water (e.g., Huntley et al., 1981; Herbers et al., 1995 a, b) are important at infragravity frequencies, and these effects are not incorporated in the models. Furthermore, the energy transfers to infragravity frequencies are sensitive to directional spreading effects that are neglected here (Herbers

et al., 1995; Herbers and Burton, 1996). Nevertheless, the roughly comparable observed and predicted infragravity energy levels suggest that nonlinear triad interactions is a plausible mechanism for the transfers of energy to infragravity frequencies in shallow water.

V. SUMMARY AND CONCLUSIONS

A stochastic model for the shoaling of waves on a beach with straight and parallel depth contours is presented, based on a third-order closure of Boussinesq equations (Herbers and Burton, 1996). The model includes nonlinear triad interactions in which two primary wave components with frequencies ω_1 and ω_2, excite a secondary wave component with the sum $(\omega_1+\omega_2)$ or difference $(\omega_1-\omega_2)$ frequency. Neglecting directional spreading effects, a coupled set of evolution equations for the wave spectrum and bispectrum is solved with standard numerical integration techniques. The model is numerically efficient and requires only an estimate of the incident wave spectrum for initialization that is often readily available from a nearby buoy or a regional wave model prediction. The bispectrum is initialized with a local prediction based on second-order finite depth theory.

Extensive numerical simulations were performed to examine the model characteristics and the dependence of wave shoaling evolution on nonlinearity, spectral shape and bottom profile. In simulations with strong nonlinearity, both narrow and broad spectra tend to evolve to a flat featureless spectrum (Figures 1f, 3f). Simulations of narrow spectra with peak frequency f_p show the familiar growth of harmonic peaks at $2fp$, $3fp$, ···. In simulations with broad spectra comparable energy transfers to higher frequencies occur, but since the interactions are spread over a wide frequency range, the spectra remain featureless (Figure 3). On gently sloping beaches predicted nonlinear energy transfer rates are weaker than on steep beaches but cause stronger cumulative

spectral evolution (Figures 1,3). On steep slopes, predicted bispectra have relatively large imaginary parts characteristic of pitched forward wave shapes, whereas the predominantly real bispectral values predicted on gentle slopes indicate symmetric wave profiles . These characteristics are qualitatively consistent with wave shape evolution observed prior to breaking on natural beaches. Simulations of waves propagating over a bar into deeper water show decreasing high-frequency spectral levels (Figure 4). The predicted bispectra indicate a reversal in nonlinear energy transfers with difference triad interactions transferring energy back towards lower frequencies.

Stochastic and deterministic (Freilich and Guza, 1984) Boussinesq model predictions were compared to extensive field observations of wave shoaling on a natural barred beach. Although predictions of the two models differ in detail, the overall agreement with the observed wave spectrum evolution is comparable. Both models predict accurately the nonlinear transfer of energy to higher frequencies for a range of incident wave conditions (Figures 7, 8, 12, 15). These results are similar to earlier studies using deterministic Boussinesq models on nearly plane California beaches (Freilich and Guza, 1984; Elgar and Guza, 1985). Although spectral levels at high frequencies generally increase as waves propagate shoreward owing to sum triad interactions, in one case a decrease in high-frequency spectral levels was observed shoreward of the sandbar, consistent with difference interactions predicted by both models (Figures 12, 13). These observations support the simulation result that energy can be transferred back to incident wave frequencies in regions of gradually increasing depth.

In conclusion, a numerically efficient stochastic Boussinesq model was developed

that predicts the evolution of wave spectra and bispectra on beaches. Comparisons of model predictions to extensive field observations from a natural beach show excellent agreement. In the future, the stochastic wave shoaling model will be extended to directionally spread waves based on similar evolution equations for the frequency-alongshore wavenumber spectrum and bispectrum (Herbers and Burton, 1996).

APPENDIX

Figure 1. Numerical simulations of the shoaling evolution of a narrow spectrum of waves (equation 7 with n = 20) over a plane beach. The model is initialized in 6 m depth. Results are shown in 4 m (upper panels), 2 m (middle panels), and 1.5 m (lower panels) depth for incident wave significant heights of 0.05 m (left panels) and 0.5 m (right panels) and beach slopes of 1:300 (solid lines) and 1:30 (dashed lines). The initial spectrum is indicated in each panel with a dotted line.

Figure 2. Normalized bispectra $b(f_1, f_2)$ (equation 8, units $Hz^{-1/2}$) predicted in 2 m depth in the simulations described in Figure 1. The real and imaginary parts of b are shown in the lower and left quadrants, respectively. Contour levels are: ± 1, 3, 5.

Figure 3. Numerical simulation of the shoaling evolution of a broad spectrum of waves (equation 6 with n = 5) over a plane beach (same format as Figure 1).

Figure 4. Simulation of the evolution of a broad spectrum (equation 6 with n = 5), with an initial H_s = 0.5 m in 6 m depth, over 3 different bottom profiles: a beach (left panels), a flat section (center panels), and a bar (right panels). Predictions are shown at x = 900, 1050, and 1200 m (indicated by asterisks in the upper panels). The dotted line indicates the initial spectrum at x = 0.

Figure 5. Normalized bispectra predicted in the simulations described in Figure 4. (a) x = 900 m (same for all 3 profiles). (b) x = 1050 m on the beach profile. (c) x = 1050 m on the flat section. (d) x = 1050 m on the bar profile. The format of the panels is the same as in Figure 2.

Figure 6. Depth profiles and sensor locations of the 4 field data case studies.

Figure 7. Comparison of observed (solid line) and predicted (asterisks = stochastic model, circles = deterministic model) spectra on September 10 at 6 instrument locations. The initial spectrum (H_s = 0.5 m) is indicated in each panel with a dashed line.

Figure 8. Comparison of observed and predicted spectra on September 15 (H_s = 0.4 m) (same format as Figure 7).

Figure 9. Cross-shore evolution of the spectral levels at the peak frequency and the first four harmonics on September 15. The solid lines are the observed levels, the dotted lines are the deterministic model predictions, and the dashed lines are the stochastic model predictions.

Figure 10. Bispectra observed (right panels) and predicted (left panels, from the stochastic model) offshore of the bar (sensor p17, upper panels) and on the bar (sensor p14, lower panels) on September 15 . The format of the panels is the same as in Figure 2.

Figure 11. Bispectra observed (right panels) and predicted (left panels, from the stochastic model) on September 15 at sensors p4 (upper panels) and p3 (lower panels), both located on the beachface close to shore. The format of the panels is the same as in Figure 2.

Figure 12. Comparison of observed and predicted spectra on September 24 (H_s = 0.8 m) (same format as Figure 7).

Figure 13. Cross-shore evolution of the spectral levels at the peak frequency and the first two harmonics on September 24 (same format as Figure 9).

Figure 14. Bispectra observed (right panels) and predicted (left panels, from the stochastic model) on the bar (sensor 14, upper panels) and inshore of the bar (sensor p23, lower panels) on September 24 . The format of the panels is the same as in Figure 2.

Figure 15. Comparison of observed and predicted spectra on September 21 (H_S = 0.8 m) (same format as Figure 7).

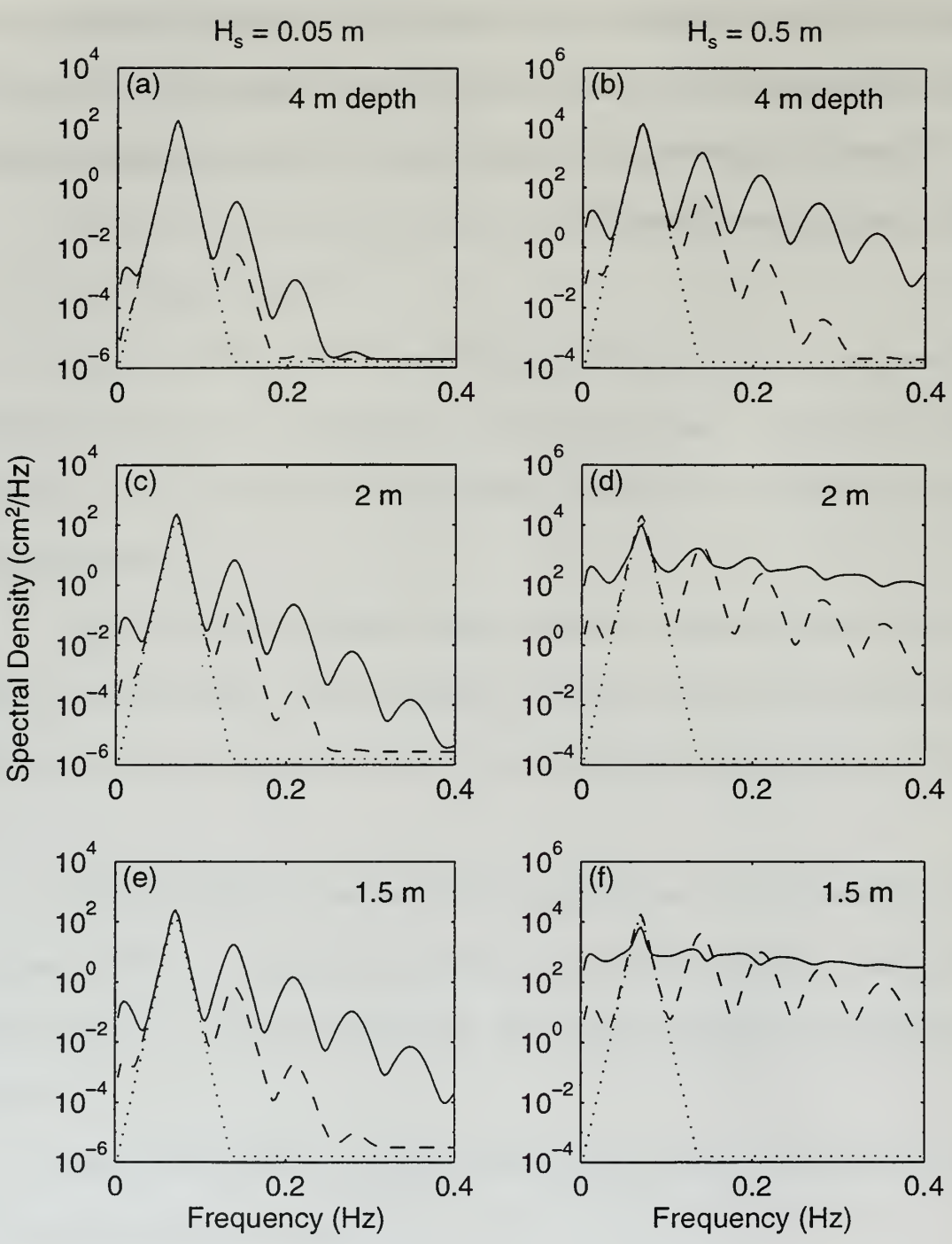
H_s = 0.05 m
H_s = 0.5 m
(a)
4 m depth
(b)
4 m depth
(c)
2 m
(d)
2 m
(e)
1.5 m
(f)
1.5 m
Spectral Density (cm²/Hz)
Frequency (Hz)
Frequency (Hz)

Figure 1

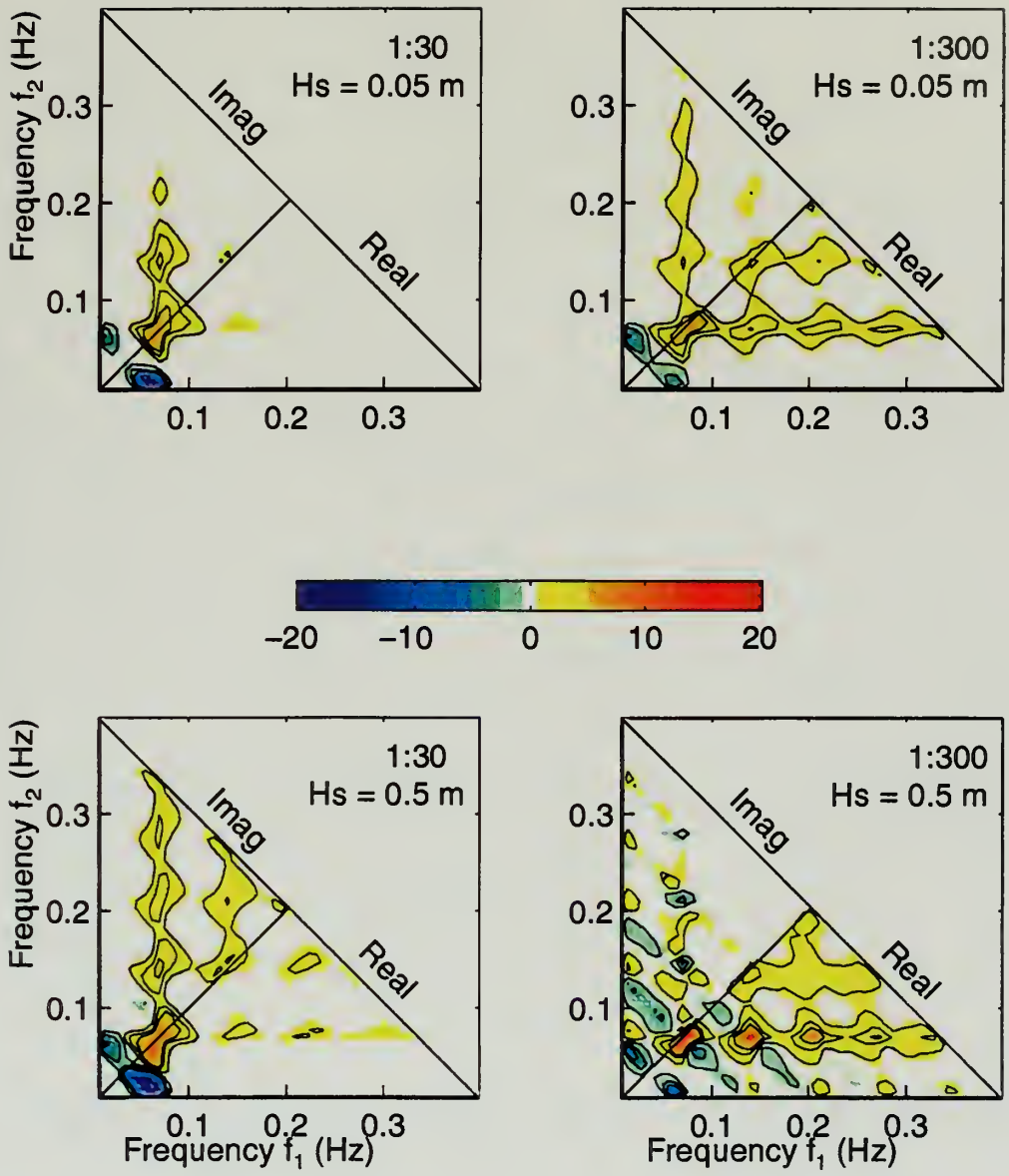
1:30
Hs = 0.05 m
Imag
Real
Frequency f2 (Hz)
0.1
0.2
0.3
1:300
Hs = 0.05 m
−20
−10
0
10
20
1:30
Hs = 0.5 m
1:300
Hs = 0.5 m
Frequency f1 (Hz)

Figure 2

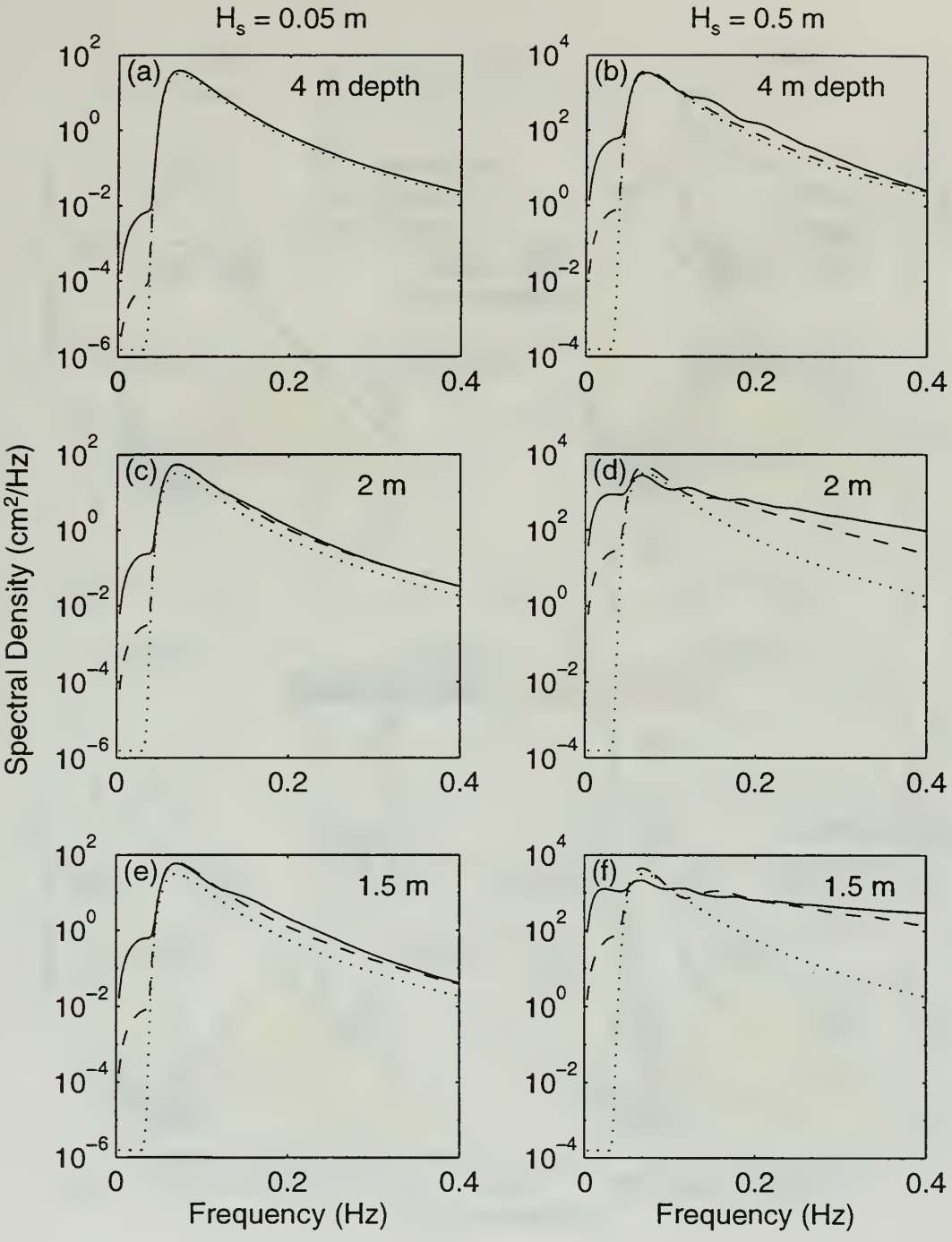
H_s = 0.05 m
H_s = 0.5 m
(a)
4 m depth
(b)
4 m depth
(c)
2 m
(d)
2 m
(e)
1.5 m
(f)
1.5 m
Spectral Density (cm²/Hz)
Frequency (Hz)
Frequency (Hz)

Figure 3

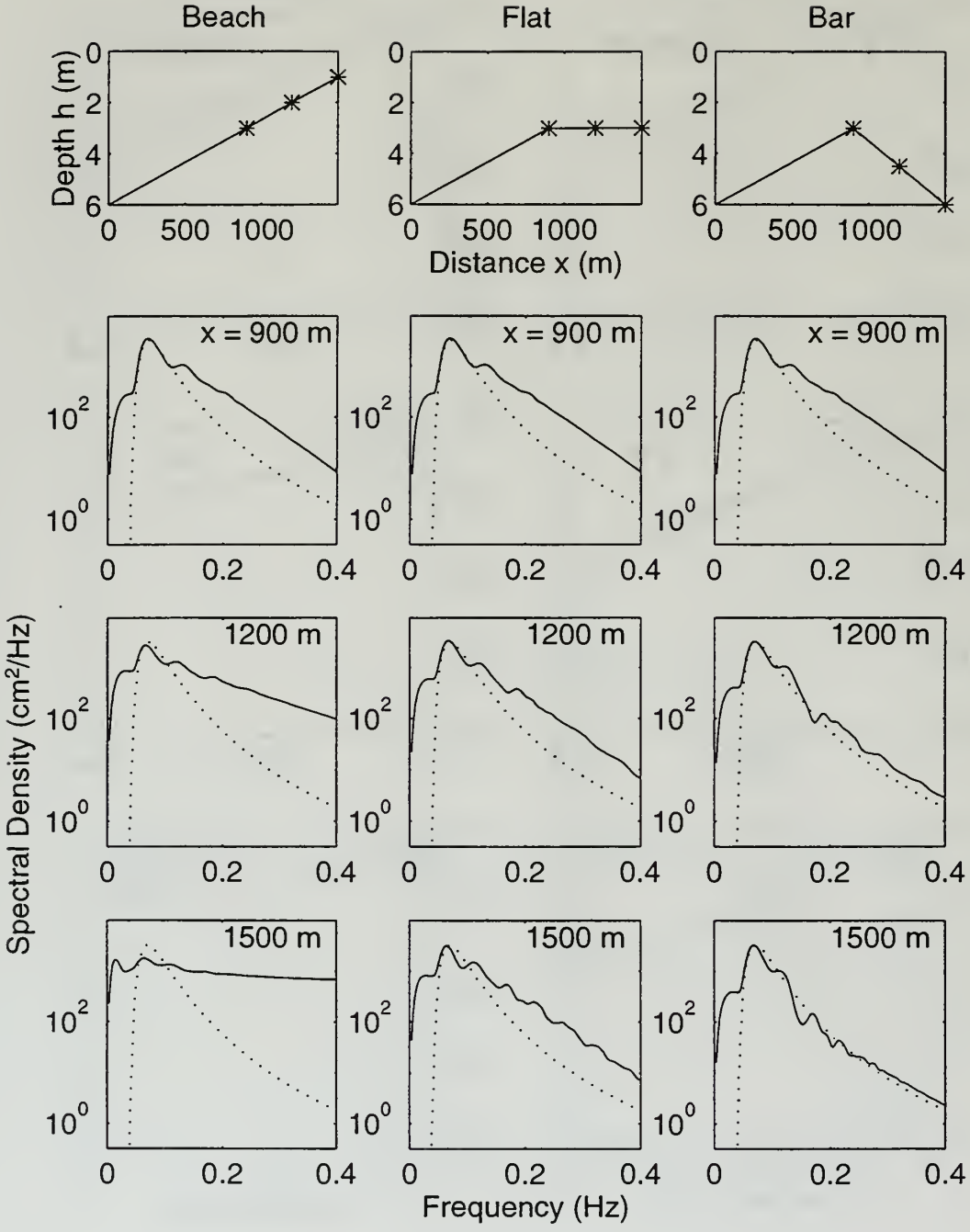
Beach
Flat
Bar
Depth h (m)
0
2
4
6
0
500
1000
Distance x (m)
x = 900 m
1200 m
1500 m
Spectral Density (cm²/Hz)
10²
10⁰
0.2
0.4
Frequency (Hz)

Figure 4

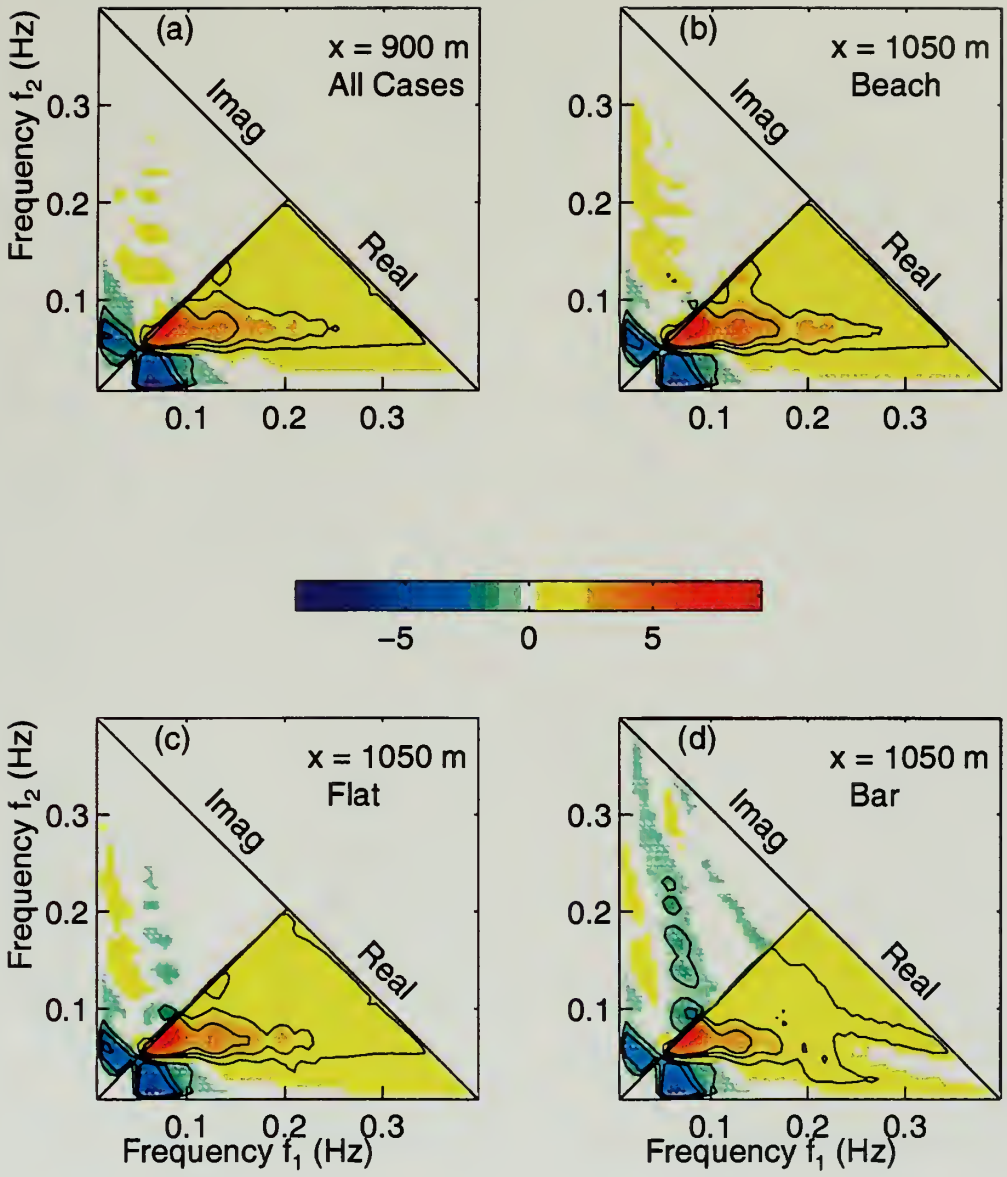
(a)
x = 900 m
All Cases
Imag
Real
(b)
x = 1050 m
Beach
(c)
x = 1050 m
Flat
(d)
x = 1050 m
Bar
Frequency f2 (Hz)
Frequency f1 (Hz)
0.1
0.2
0.3
−5
0
5

Figure 5

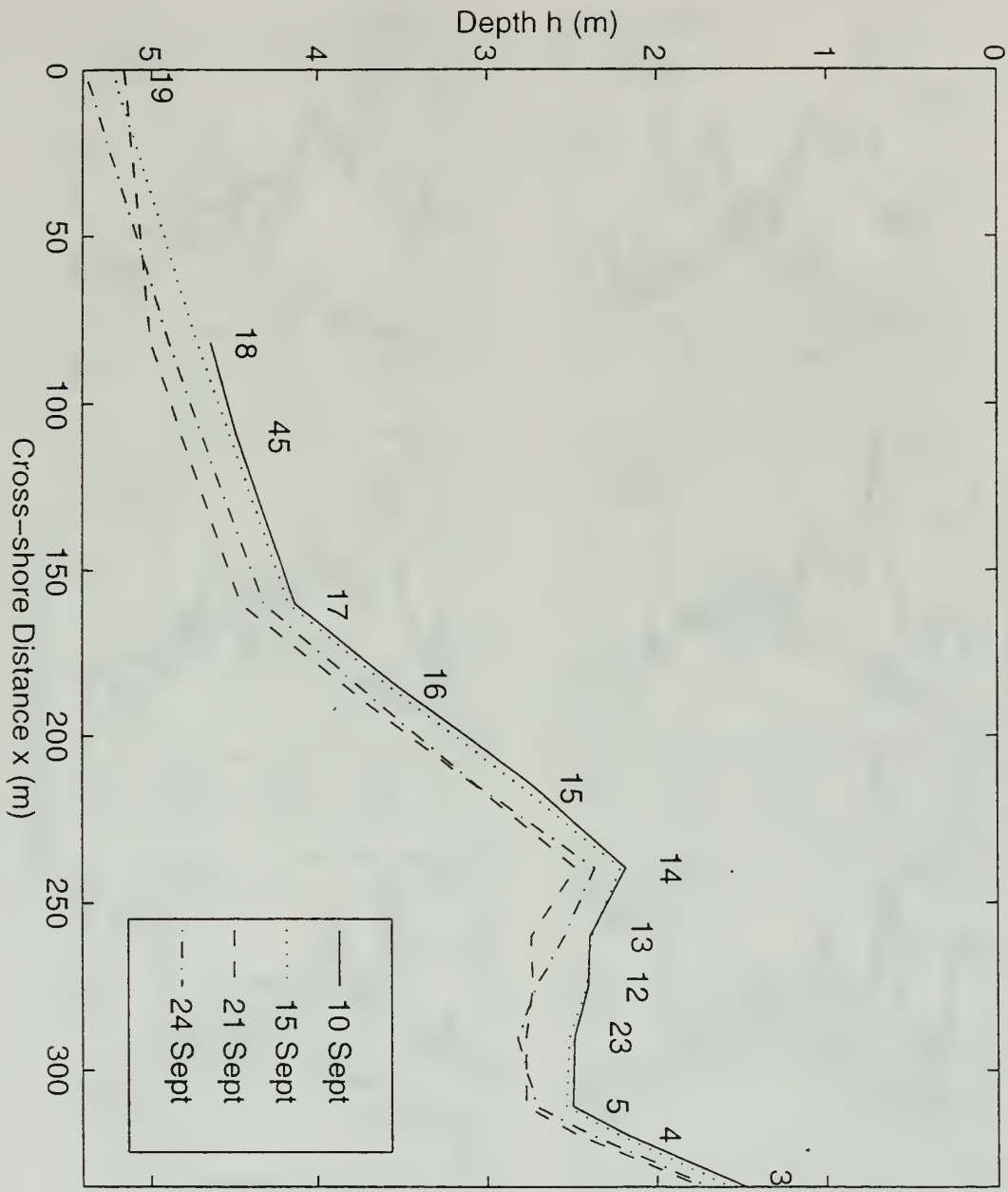
Depth h (m)
Cross-shore Distance x (m)
0
1
2
3
4
0
50
100
150
200
250
300
19
5
18
45
17
16
15
14
13
12
23
5
4
3
10 Sept
15 Sept
21 Sept
24 Sept

Figure 6

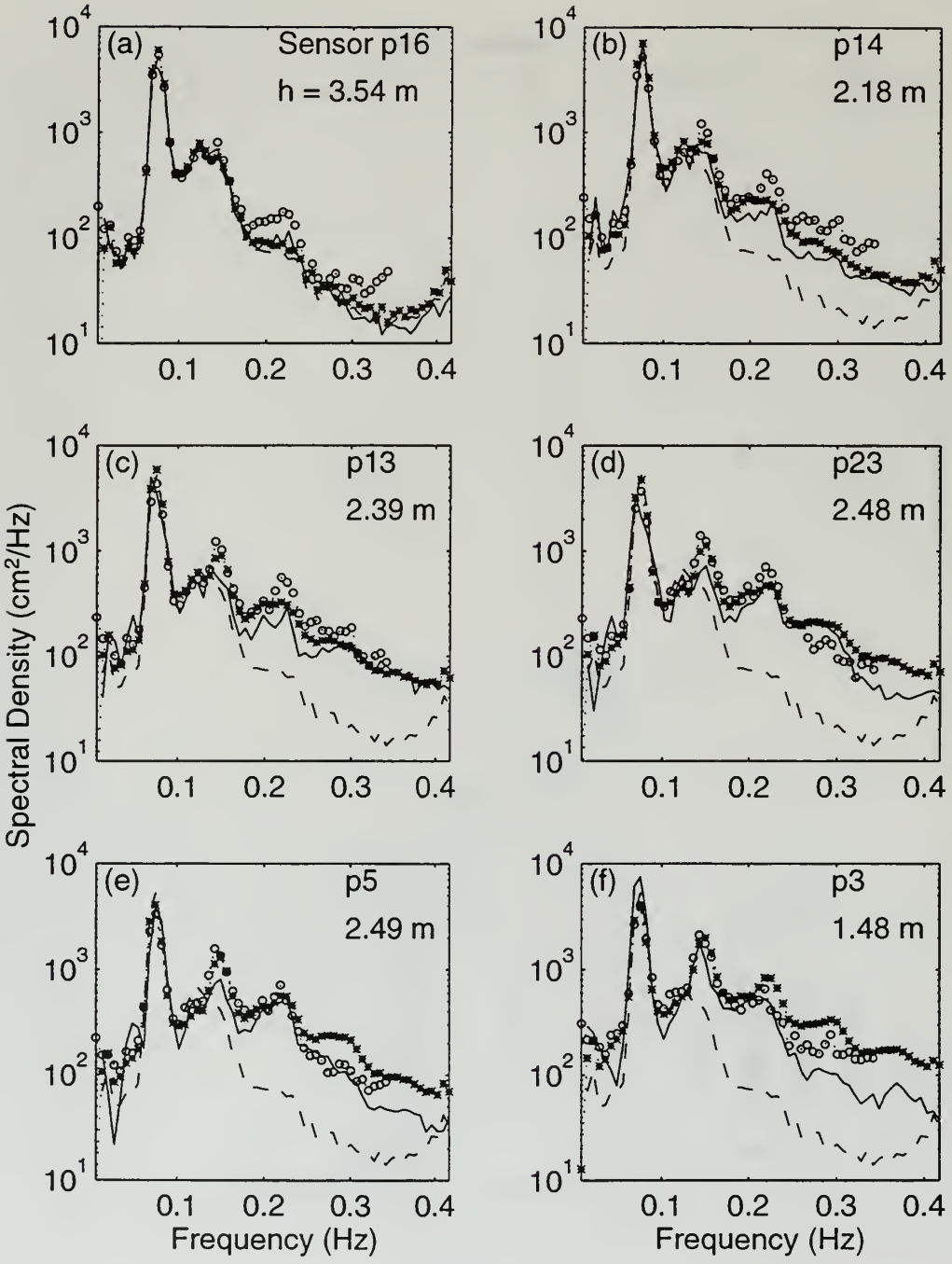
(a)
Sensor p16
h = 3.54 m
(b)
p14
2.18 m
(c)
p13
2.39 m
(d)
p23
2.48 m
(e)
p5
2.49 m
(f)
p3
1.48 m
Spectral Density (cm²/Hz)
Frequency (Hz)
Frequency (Hz)

Figure 7

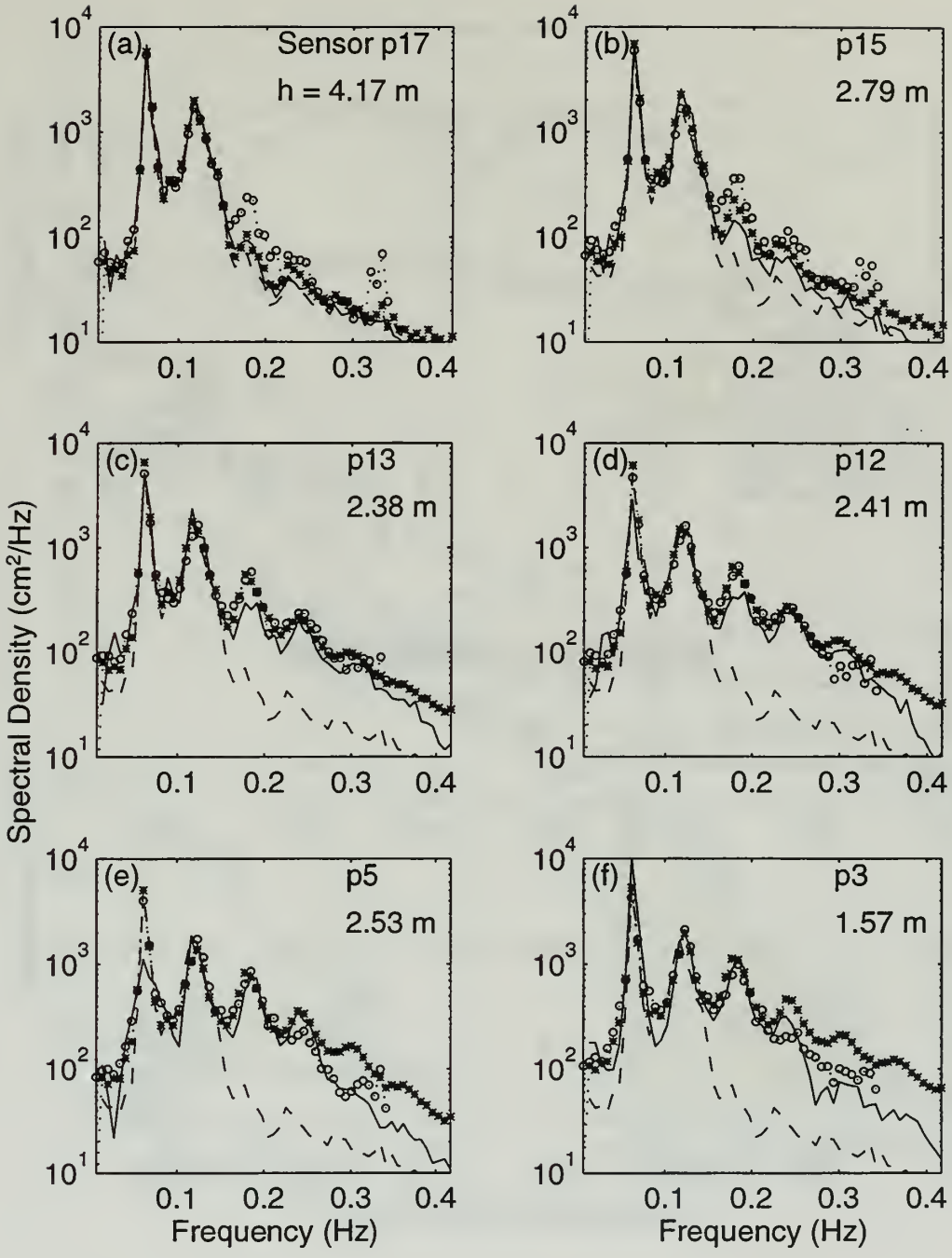
(a)
Sensor p17
h = 4.17 m
(b)
p15
2.79 m
(c)
p13
2.38 m
(d)
p12
2.41 m
(e)
p5
2.53 m
(f)
p3
1.57 m
Spectral Density (cm²/Hz)
Frequency (Hz)
Frequency (Hz)

Figure 8

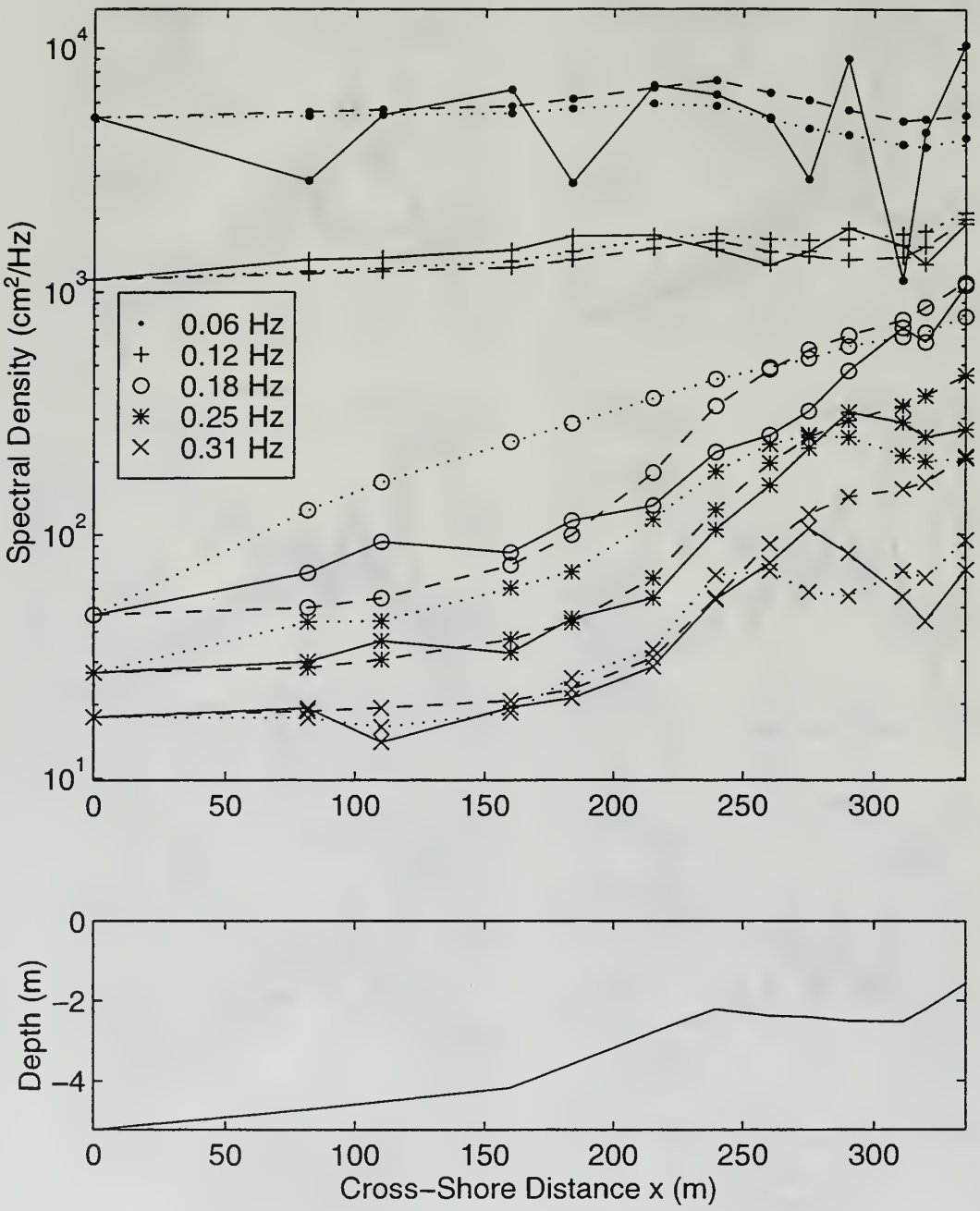
Spectral Density (cm²/Hz)
10⁴
10³
10²
10¹
0.06 Hz
0.12 Hz
0.18 Hz
0.25 Hz
0.31 Hz
0
50
100
150
200
250
300
Depth (m)
0
−2
−4
Cross−Shore Distance x (m)

Figure 9

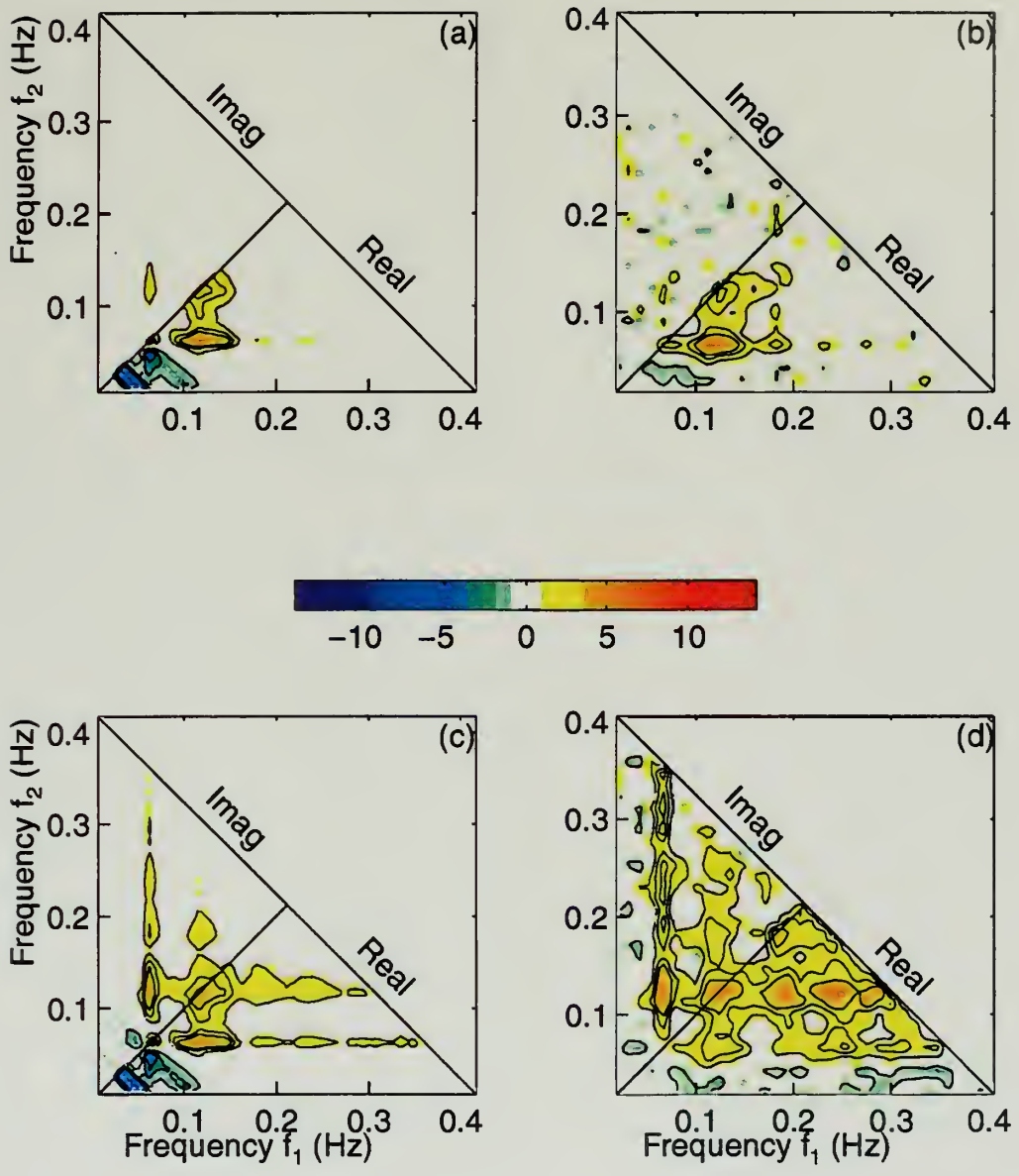
(a)
(b)
(c)
(d)
Imag
Real
Frequency f_2 (Hz)
Frequency f_1 (Hz)
0.1
0.2
0.3
0.4
−10
−5
0
5
10

Figure 10

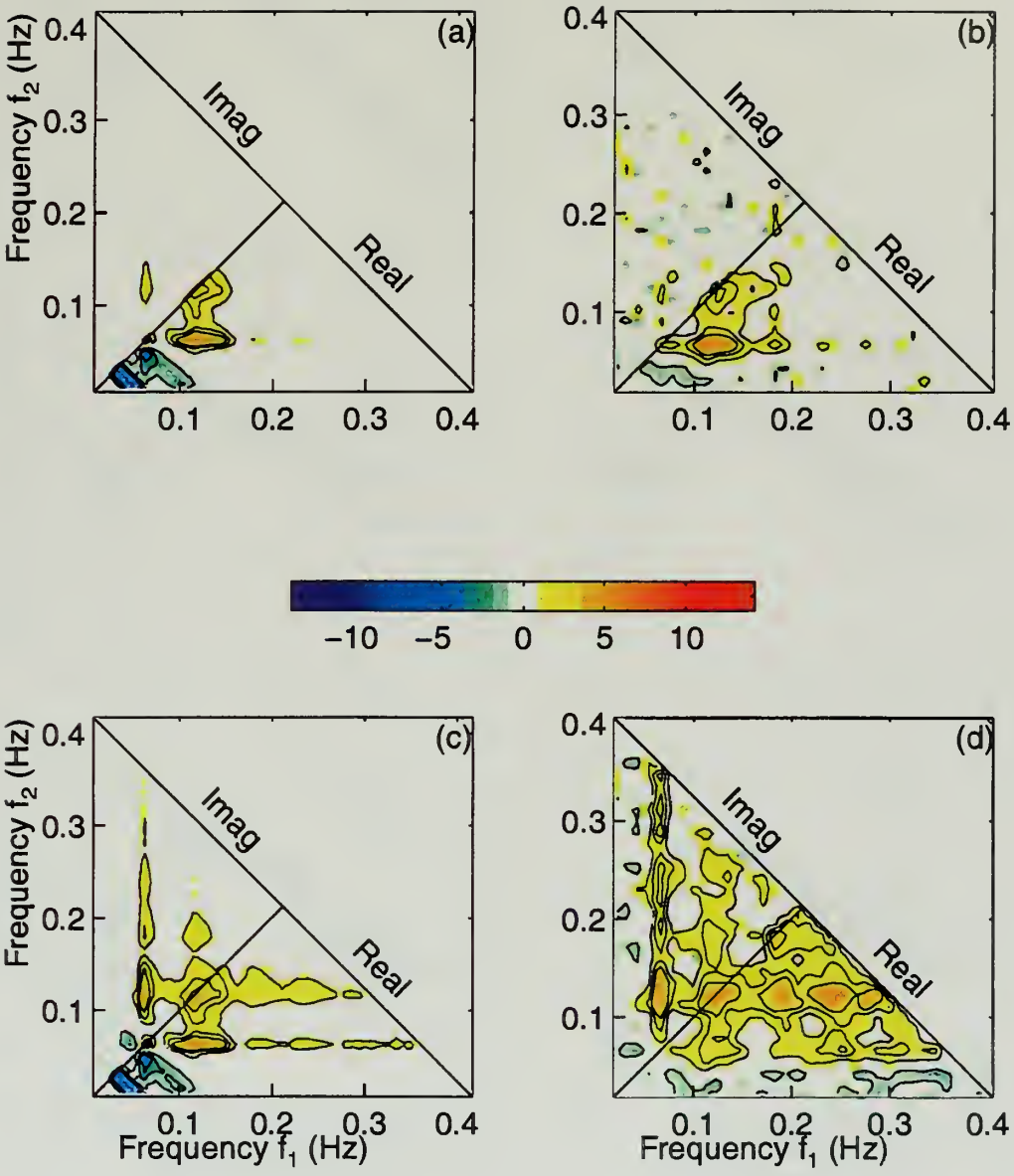
(a)
(b)
(c)
(d)
Imag
Real
Frequency f_2 (Hz)
Frequency f_1 (Hz)
0.1
0.2
0.3
0.4
−10
−5
0
5
10

Figure 11

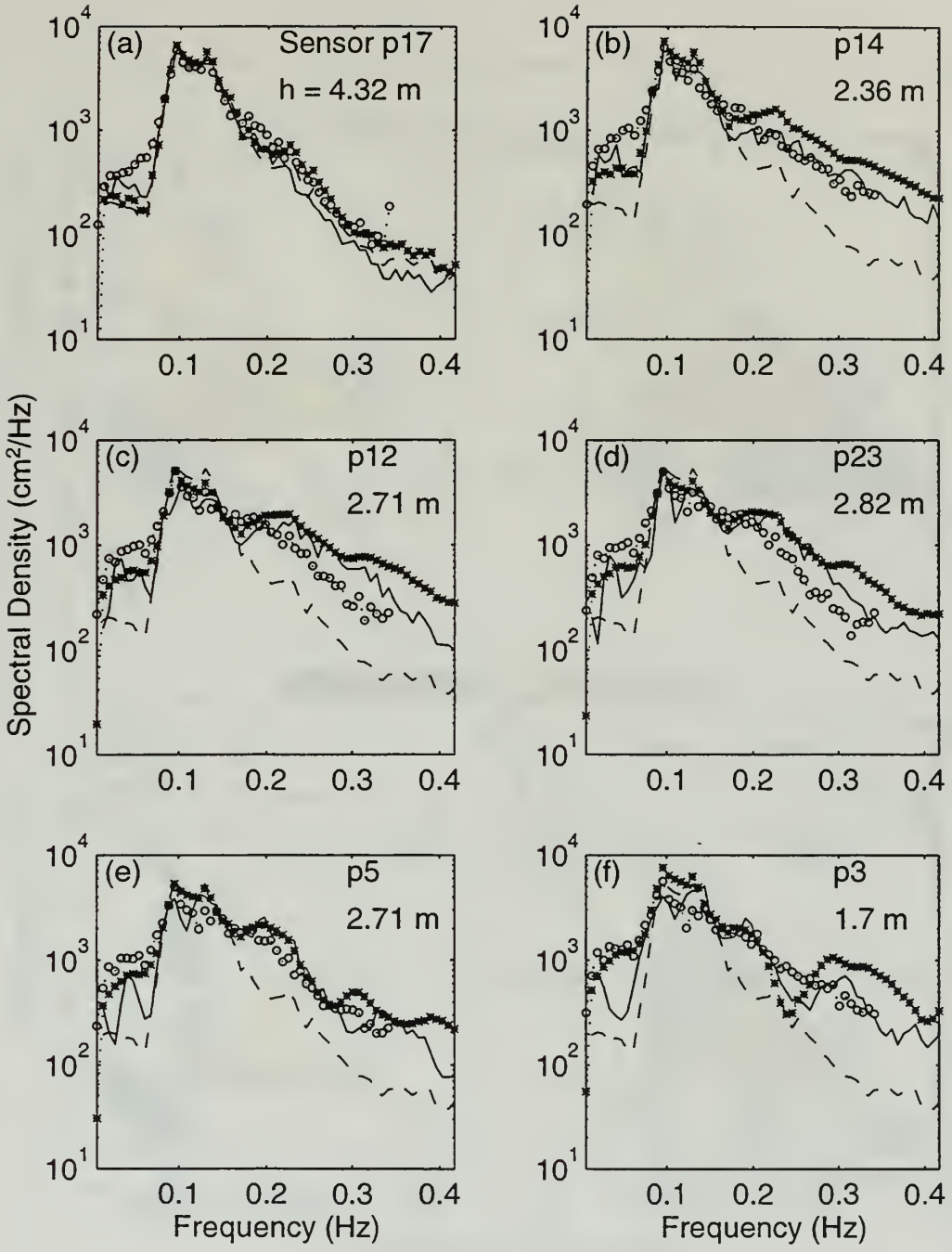
(a)
Sensor p17
h = 4.32 m
(b)
p14
2.36 m
(c)
p12
2.71 m
(d)
p23
2.82 m
(e)
p5
2.71 m
(f)
p3
1.7 m
Spectral Density (cm²/Hz)
Frequency (Hz)
Frequency (Hz)

Figure 12

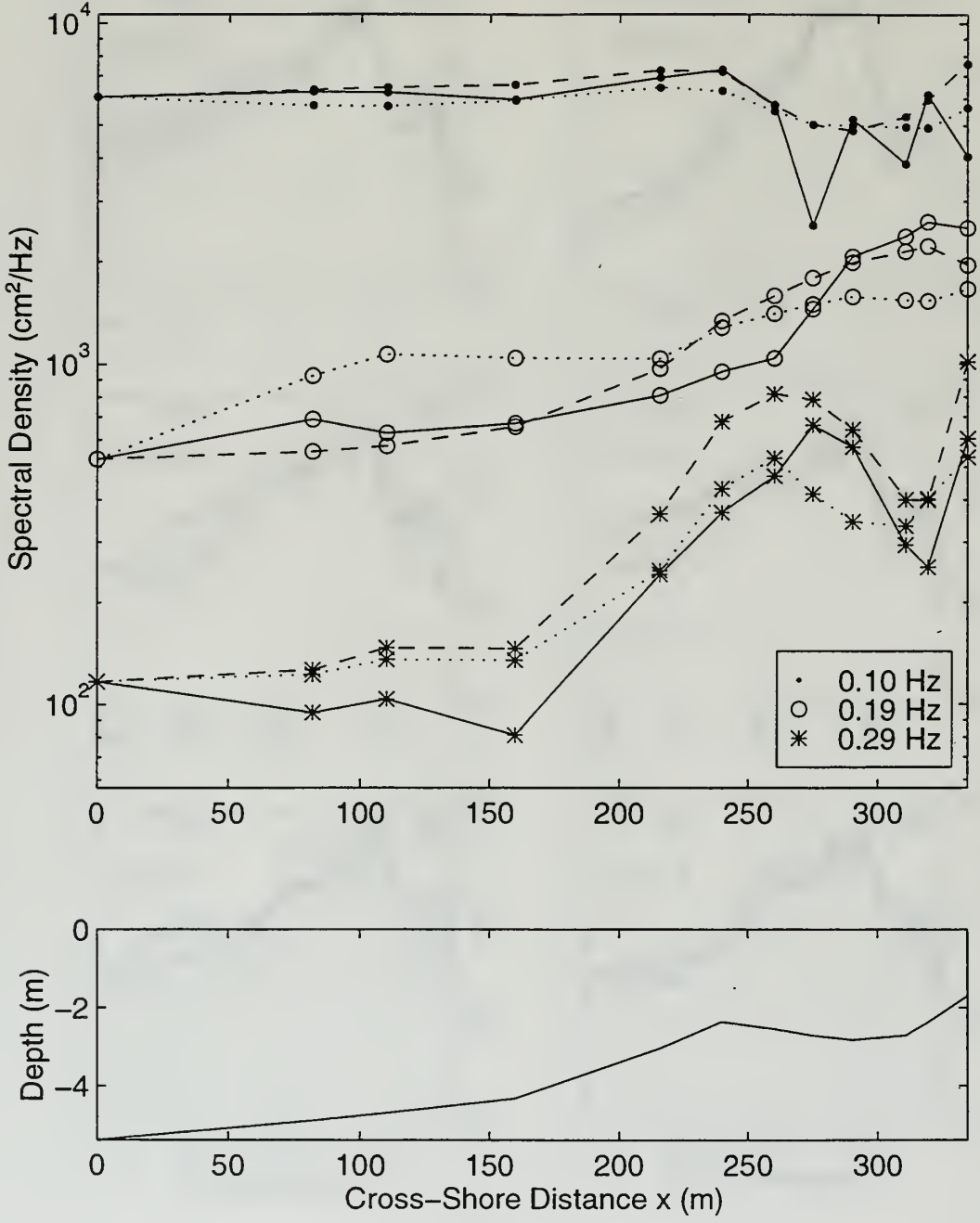
Spectral Density (cm²/Hz)
10⁴
10³
10²
0.10 Hz
0.19 Hz
0.29 Hz
0
50
100
150
200
250
300
Depth (m)
0
−2
−4
Cross−Shore Distance x (m)

Figure 13

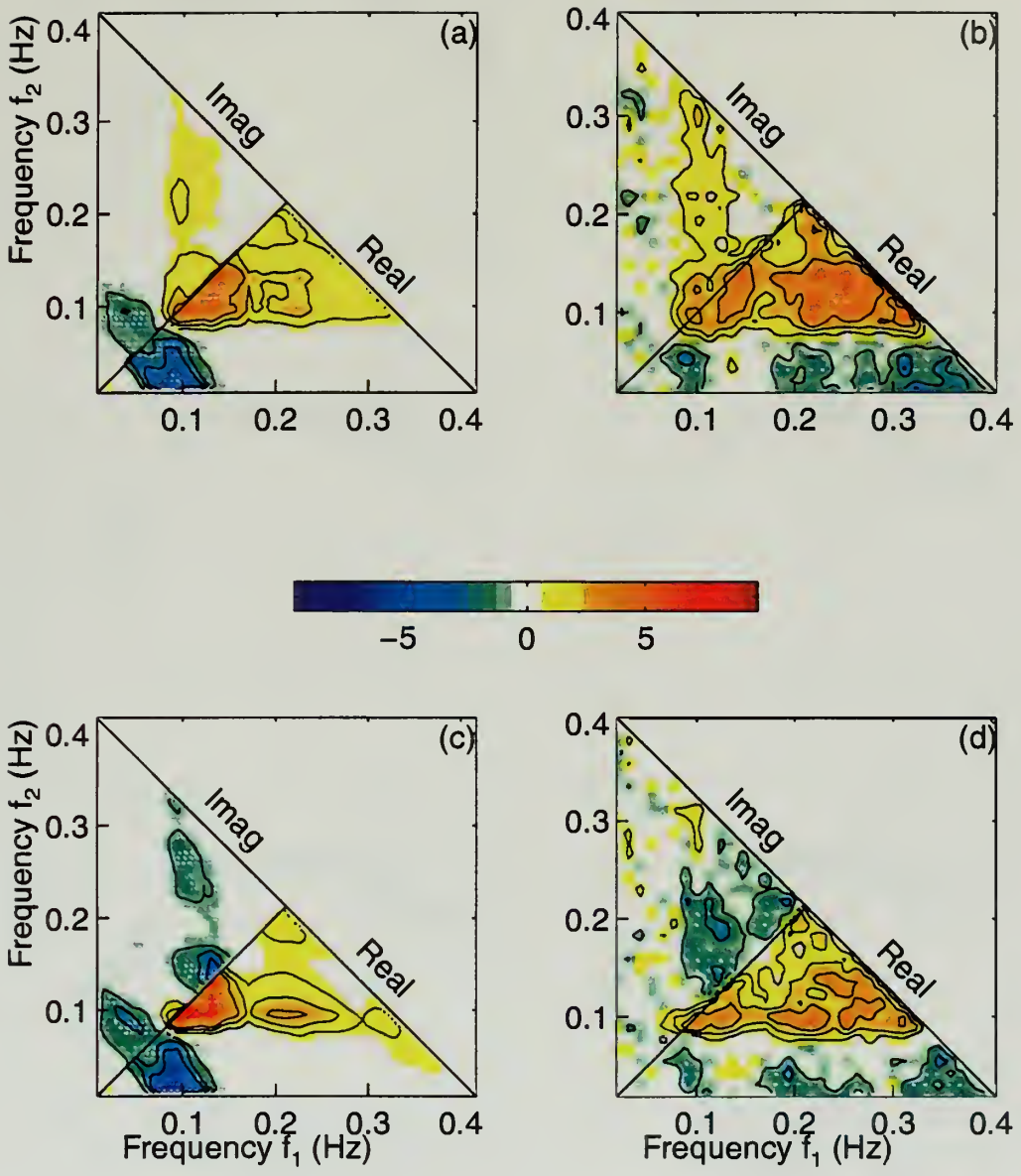

Figure 14

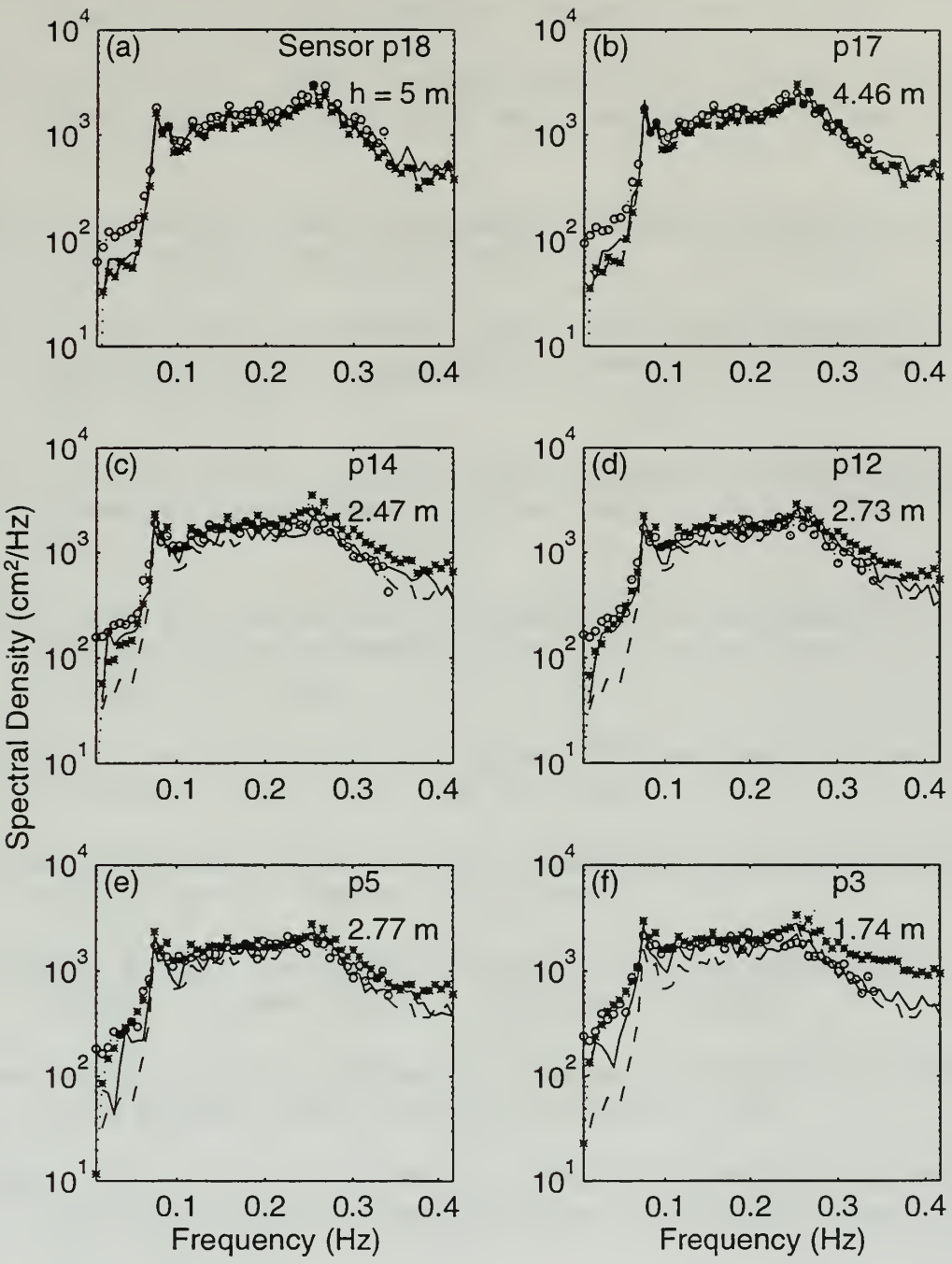
(a) Sensor p18
h = 5 m
(b) p17
4.46 m
(c) p14
2.47 m
(d) p12
2.73 m
(e) p5
2.77 m
(f) p3
1.74 m
Spectral Density (cm²/Hz)
Frequency (Hz)
Frequency (Hz)

Figure 15

LIST OF REFERENCES

Bulirsch, R. and Stoer, J., 1966, "Numerical Treatment of Ordinary Differential Equations by Extrapolation Methods", *Numerische Math.*, 8, 1-13.

Elgar, S. and Guza, R.T., 1985a, "Shoaling Gravity Waves: Comparisons Between Field Observations, Linear Theory, and a Nonlinear Model", *J. Fluid Mech.*, 158, 47-70.

Elgar, S. and Guza, R.T., 1985b, "Observations of Bispectra of Shoaling Surface Gravity Waves", *J. Fluid Mech.*, 161, 425-448.

Elgar, S., Freilich, M.H. and Guza, R.T., 1990a, "Model-Data Comparisons of Moments of Nonbreaking shoaling Surface Gravity Waves", *J. Geophys. Res.*, 95, 16055-16063.

Elgar, S., Freilich, M.H. and Guza, R.T., 1990b, "Recurrence in Truncated Boussinesq Models for Nonlinear Waves in Shallow Water", *J. Geophys. Res.*, 95, 11547 - 11556.

Elgar, S., Guza, R.T., Raubenheimer, B., Herbers, T. H. C. and Gallagher, E. L., 1996, "Spectral Evolution of Shoaling and Breaking Waves on a Barred Beach", *J. Geophys. Res.*, in press.

Freilich, M.H. and Guza, R.T., 1984, "Nonlinear Effects on Shoaling Surface Gravity Waves", *Phil. Trans. R. Soc. Land*, A311, 1-42.

Gallagher, E.L., Elgar, S., Guza, R.T., 1997, "Observations of Sand Bar Evolution on a Natural Beach", *J. Geophys. Res.*, submitted.

Hasselmann, K., 1962, "On the Nonlinear Energy Transfer in a Gravity-Wave Spectrum, 1, General Theory", *J. Fluid Mech.*, 12, 481-500.

Hasselmann, K., Munk, W., MacDonald, G., "Bispectra of Ocean Waves", **Time Series Analysis**, Chap. 8, John Wiley & Sons, Inc., 1963.

Herbers, T.H.C., Lowe R.L. and Guza, R. T., 1992, "Field Observations of Orbital Velocities and Pressure in Weakly Nonlinear Surface Gravity Waves", *J. Fluid Mech.*, 245, 413-435.

Herbers, T.H.C., Elgar, S., and Guza, R.T., 1994, "Infragravity-frequency (0.005-0.05 Hz) Motions on the Shelf, Part I: Forced Waves", *J. Phys. Oceanogr.*, 24, 917-927.

Herbers, T.H.C. and Burton M.C., 1996, "Nonlinear Shoaling of Directionally Spread Waves on a Beach", *J. Geophys. Res.*, submitted.

Herbers, T.H.C., Elgar, S., and Guza, R.T., 1995, "Generation and Propagation of Infragravity Waves", *J. Geophys. Res.*, 100(C12), 24863-24872.

Peregrine, D.H., 1967, "Long Waves on a Beach", *J. Fluid Mech.*, 27, Part 4, 815-827.

Phillips, O.M., 1960, "On the Dynamics of Unsteady Gravity Waves of Finite Amplitude, Part 1, The Elementary Interactions", *J. Fluid Mech.*, 9, 193-217.

Pierson, W.J.,Jr. and Moskowitz, L., 1964, "A Proposed Spectral Form for Fully Developed Wind Seas Based on the Similarity Theory of S.A. Kitaigorodskii", *J. Geophys. Res.*, 69, 5181.

Press, W.H., et al., **Numerical Recipes in Fortran: The Art of Scientific Computing**, 2nd ed., Cambridge University Press, 1992.

Ursell, F., 1953, "The Long-wave Paradox in the Theory of Gravity Waves", *Proc. Camb. Phil. Soc.*, 49, 685-694.

WAMDI Group, 1988, "The WAM Model: A Third Generation Ocean Wave Prediction Model", *J. Phys. Oceanogr.*, 18, 1775-1810.

INITIAL DISTRIBUTION LIST

	No. Copies
1. Defense Technical Information Center 8725 John J. Kingman Rd., STE 0944 Ft. Belvoir, VA 22060-6218	2
2. Dudley Knox Library Naval Postgraduate School 411 Dyer Rd. Monterey, CA 93943-5101	2
3. Professor T.H.C. Herbers, Code OC/He Department of Oceanography Naval Postgraduate School Monterey, CA 93943 - 5121	8
4. Professor E.B. Thornton, Code OC/Tm Department of Oceanography Naval Postgraduate School Monterey, CA 93943 - 5121	1
5. Professor Gragg, Code MA/Gr Department of Mathematics Naval Postgraduate School Monterey, CA 93943 - 5121	1
6. Craig Noheim 908 Bluewater Drive Indian Harbour Beach, FL 32937	1